Int. J. Electrochem. Sci., 11 **(2016)** 5552 – 5563, doi: 10.20964/2016.07.64

International Journal of
ELECTROCHEMICAL
SCIENCE
www.electrochemsci.org

Electrochemical and Mechanical Properties of Cast Ti-V Alloys for Dental Applications

Kyung Hee Park, Moon-Jin Hwang, Ho-Jun Song and Yeong-Joon Park[*]

Department of Dental Materials and Medical Research Center for Biomineralization Disorders, School of Dentistry, Chonnam National University, Gwangju 61186, Korea
[*]E-mail: yjpark@jnu.ac.kr

Received: 6 April 2016 / *Accepted:* 12 May 2016 / *Published:* 4 June 2016

A series of Ti-*x*V alloys with a vanadium (V) content ranging from 5 to 20 wt% were fabricated to investigate phase/microstructure, various mechanical, and electrochemical properties. The microstructural samples were characterized using X-ray diffractometry (XRD), scanning electron microscopy (SEM) and transmission electron microscopy (TEM). All the Ti-*x*V alloys showed colonies of hexagonal close packed (hcp) α-phase lamellae within large body centered cubic (bcc) β-phase grains of several lath boundaries. As a result of solid-solution strengthening of α-Ti and β-Ti phase matrix, the Ti-*x*V showed better mechanical properties than the commercially pure titanium (cp-Ti). Based on the electrochemical results, the Ti-5V alloy exhibited improved corrosion resistance as compared with cp-Ti.

Keywords: Ti-V alloy, mechanical properties, electrochemical properties, dental materials

1. INTRODUCTION

Commercially pure titanium (cp-Ti) has an established reputation because of its low density, high resistance to corrosion and excellent biocompatibility for dental prosthetic applications including partial frameworks and dental implants [1-3]. Titanium and its alloys show good corrosion resistance in various media, such as acids, alkalis, organic compounds, and chlorine media. In recent years, attempts were made to develop β type titanium alloys with mechanical compatibility, and low elastic modulus [4]. Whereas pure titanium is a monophasic, physiologically inert, and nontoxic metal, titanium alloys that contain vanadium as a β-stabilizing element have α+β phase structure with attractive mechanical properties.

Ti-6Al-4V is one of the most commonly used α-β titanium alloy due to its favorable combination of physical and mechanical properties. Vanadium known mainly for enhancing mechanical properties of alloy steels in the metal industry, has also been recognized as a trace element essential for biological activity in most living animals [5]. However, some researchers have expressed reservations concerning the presence of elements such as vanadium in long-term implants because of their toxicity both in the elemental state and oxides [6,7]. Although a role for vanadium in bone formation has been demonstrated [8,9], its mechanisms of action have remained largely unexplored. Vanadium and titanium-vanadium (Ti-V) alloys are much lighter than most refractory metals. This property makes vanadium a logical choice for applications in which strength-to-weight ratios are important, such as in the aerospace and aircraft industries. Of all the refractory alloys, vanadium alloys have the highest strength-to-weight ratios. At room temperature, vanadium and its alloys have excellent corrosion resistance in salt water and dilute hydrochloric acid, and good corrosion resistance in sodium hydroxide solutions [10].

We analyzed the effect of influence of lamellar microstructure on the mechanical properties of selected two-phase titanium alloys. The corrosion resistance of titanium was improved by the addition of a small amount of vanadium as the enhanced cathodic reaction promotes the active-passive transition. The goal of this study was to evaluate and compare mechanical, microstructures and the electrochemical corrosion behavior of cp-Ti and Ti-*x*V alloys.

2. EXPERIMENTAL

2.1. Preparation of materials

A commercially-available cp-Ti (ASTM Grade II, Daito Steel, Tokyo, Japan) was used as a control titanium material. A series of binary Ti-*x*V (x = 5, 10, 15, and 20 wt%) were prepared by arc-melting the stoichiometric quantities of the elements on a water-cooled copper hearth using a tungsten electrode in a highly pure argon atmosphere. The starting materials (99.9% Ti sponge and 99.7% vanadium pieces) (Alfa Aesar, Ward Hill, MA, USA) were used without purification. During the arc-melting procedure, a titanium getter was melted prior to melting the reactant mixture to further purify the argon atmosphere. The ingots were inverted and remelted seven times to ensure compositional homogeneity. Subsequently, the samples were heat treated using a tube furnace in argon atmosphere for 4 h at temperatures that was 150°C lower than their respective solidus temperatures followed by cooling down to 600°C in a furnace at a rate of 10°C/min and air-cooling to room temperature. These heat-treatment conditions were chosen in accordance with the binary Ti-V phase diagrams [11].

2.2. Characterization of Ti-xV alloys

The phase constitutions were identified by X-ray diffraction (XRD) analysis using a X'Pert PRO Multi–Purpose X-Ray Diffractometer (40 kV and 40 mA, PANalytical B.V., Almelo, Netherlands) with Cu Kα (λ = 1.54056 Å). Intensities of the XRD were obtained in the 2θ range

between 20° and 80° with a step size of 0.02°/3 s. The microstructure was examined by scanning electron microscopy (SEM, Hitachi S-3000N, Japan) at 15 kV. The chemical compositions were examined by energy dispersive X-ray analysis (EDX, EMAX, Horiba, Japan) at 20 kV. The phase structures were identified by high resolution transmission electron microscopy (HR-TEM, Technai-F20, Philips, Amsterdam, Netherlands) and selected area electron diffraction (SAED).

2.3. Mechanical properties of specimens

The microhardness of polished alloys was measured using a Vickers microhardness tester (Zwick, Postfach4350, Ulm, Germany) with a load of 500 g for 30 s. Elastic modulus was measured for each material using an acoustic impulse excitation apparatus (Grindosonic MK5, J.W. Lemmens, MO, USA) from the resonance frequency as described in ASTM C1259-08e1.

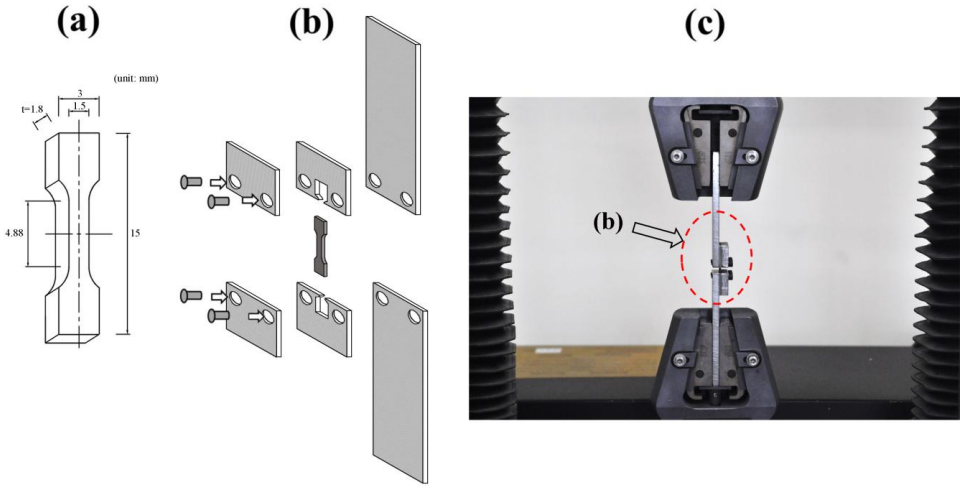

Figure 1. Tensile test specimen and grip designs; (a) dumbbell-shaped tensile test specimen, (b) specially fabricated grip assembly, and (c) tensile test image using grip assembly.

A flexure wave is sent through a rectangular bar of length *L*, width *w*, thickness *t*, and mass *m*. The frequency of the flexure wave (f_f) can be detected using a piezoelectric transducer and then used in Equation (1) to determine elastic modulus (E) where T_1 is a correction factor defined in the standard. The reported values are averages of the obtained data and errors are the standard deviation.

$$E = 0.9465\left(\frac{m{f_f}^2}{w}\right)\left(\frac{L^3}{t^3}\right)T_1 \qquad (1)$$

The ultimate tensile strength was evaluated by a universal testing machine (Instron 4302, Instron Co., Ltd., USA) at cross-head speed of 1.5 mm/min. As shown in Figure 1(a), the tensile test specimens were prepared in a dumbbell-shape. Dumbbell-shaped test specimen was prepared in a reduced form of the dumbbell-shaped test specimen dictated in the ISO 9693 standard [12]. To evade an unnecessary preload to the sample, we used a specially fabricated grip assembly (Figure 1b), made

of high grade carbon tool steel. Dumbbell-shaped specimen was inserted into the dumbbell-head-shaped slots of the upper- and lower-grip faces, and those were secured to the tensile loading bar using cover plates and screws. While the cross-head moves upward, a vertical tensile load is applied to the dumbbell head of the specimen.

2.4. Electrochemical measurements

The samples with an approximately 10-mm diameter were mechanically polished with silicon carbide paper of up to #2000 grit and cleaned in acetone and ethanol. The electrochemical measurements were performed using the three electrode configuration consisting of the test samples working electrode, the high-density graphite counter electrode, and a saturated calomel reference electrode (SCE) as per ASTM G5-94 standard [13]. Argon gas was bubbled through the electrolyte at 150 mL/min for more than 20 minutes to degas the residual oxygen prior to the start of each experiment. For all experiments, fresh electrolyte was used. The samples were placed in a holder made of Teflon and an area of 0.283 cm^2 was exposed to the electrolyte. After immersion of the test sample in the electrolyte, the open circuit potential for 1 h was recorded. The potentiodynamic anodic polarization test was conducted at a scan rate of 5 mV/s from −1.5 to +1.5 V (vs. SCE) using a potentiostat (WAT 100, WonA Tech., Seoul, Korea) in 0.9% NaCl solution at 37 ± 1°C. At least three samples were tested to confirm experimental results. The potentiodynamic polarization curves were plotted using an automatic data acquisition system. Corrosion potential and current density were estimated by Tafel plots using both anodic and cathodic branches. The corrosion rate was determined using corrosion parameters obtained from the Tafel extrapolation method.

Electrochemical impedance measurement was performed according to the ASTM G106-89 [14]. The AC impedance spectra were obtained in the frequency range of 10^5 to 0.01 Hz with an amplitude of 10mV, using a ZIVE SP2 instrument (WonA Tech., Korea). The optimized equivalent circuit was obtained by a non-linear least-squares fitting. The parameters of equivalent circuit were calculated using ZMAN 2.2 software.

The galvanic current densities of various Ti-*x*V/cp-Ti galvanic pairs were measured over a 20-minute period by a potentiostat/galvanostat at ambient conditions (ZIVE SP2). The experimental setup for electrochemical measurements consisted of a three-electrode cell with the sample as a working electrode with an exposed area of 0.785 cm^2, an SCE as the reference electrode and cp-Ti as the counter electrode.

3. RESULTS AND DISCUSSION

We analyzed the XRD patterns to characterize the phases of the cast alloy. The phases were identified by matching each characteristic peak with the Joint Committee on Powder Diffraction Standards (JCPDS) files. Figure 2 shows the XRD patterns of cp-Ti and the series of binary Ti-*x*V alloys. The cp-Ti showed a hexagonal closed-packed crystal, a phase structure in which the unit cell

constants were a = 2.959(1) Å and c = 4.703 Å (c/a ratio = 1.589), corresponding well with those in the literature (JCPDS # 44-1294) [15].

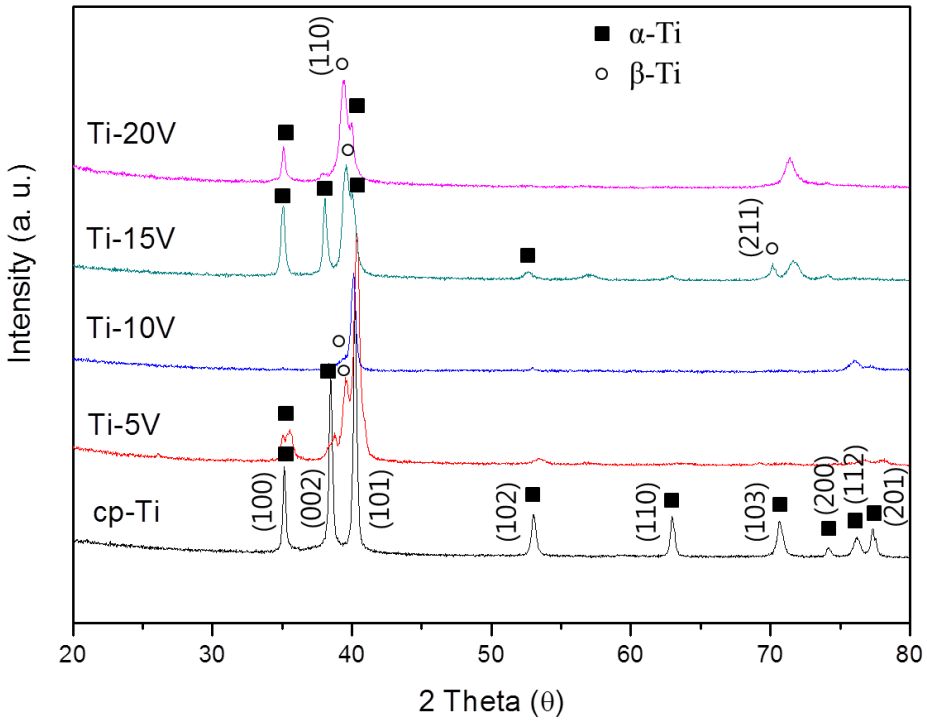

Figure 2. XRD patterns of the cast cp-Ti and the series of binary Ti-*x*V (*x* = wt% of vanadium).

These results revealed that the phase/crystal structure of the binary Ti-*x*V alloy was sensitive to the vanadium content in the cast alloy. When 5 wt% vanadium was added, all the diffraction peaks matched the α-Ti structure, and the unit cell constants calculated from the diffraction peaks were a = 2.957(1) Å and c = 4.696(1) Å (c/a ratio = 1.588), indicating the formation of a solid solution between titanium and vanadium. We observed that the addition of vanadium didn't cause a noticeable shift in the XRD peaks which might be explained by the small atomic radius difference between Ti (1.45 Å) and V (1.34 Å) [16]. However, it should be noted that the weak shoulder peak was observed at 2θ value of about 39°, indicating the presence of β phase (110). When vanadium was added to the titanium, the XRD profile showed coexistence of α and β phases. The additional peaks at 2θ values of 39° and 72° indicated the presence of the β-Ti phase. When the alloy contained 15 wt% or more vanadium, β-Ti phase could be observed distinctly in alloys.

To investigate the influence of the addition of vanadium on the microstructures of titanium, we observed the samples under a scanning electron microscope (SEM). Figure 3 shows the microstructures of Ti-*x*V alloys with different vanadium contents (5, 10, 15, and 20 wt%).

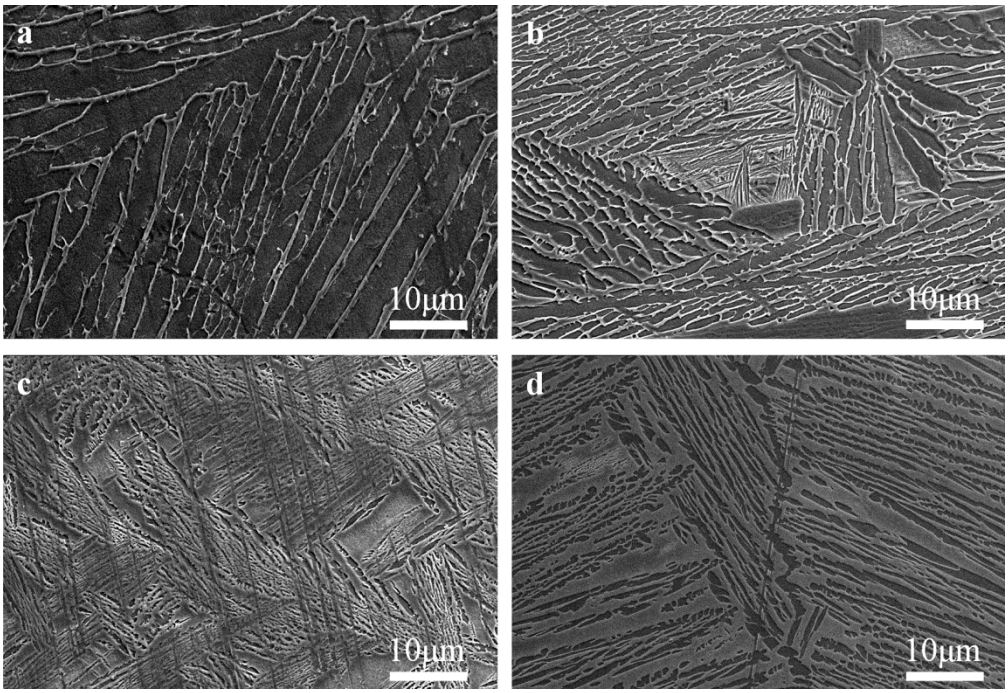

Figure 3. Scanning electron micrographs of Ti-*x*V alloys; (a) Ti-5V, (b) Ti-10V, (c) Ti-15V, and (d) Ti-20V.

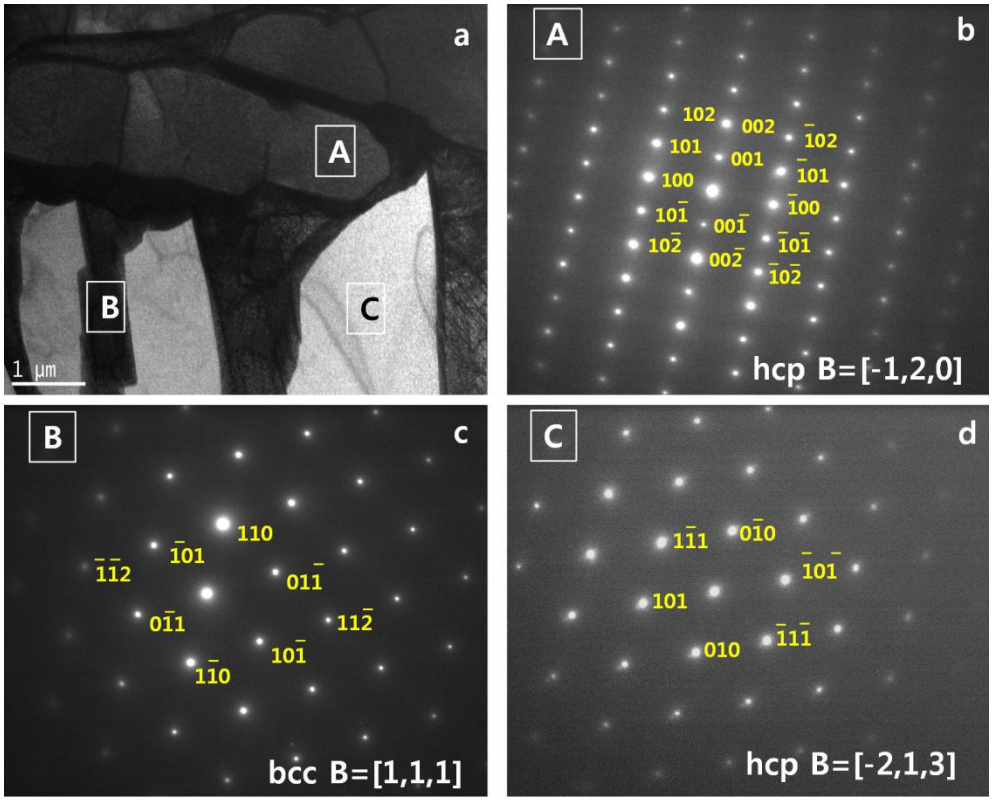

Figure 4. Transmission electron micrograph of Ti-10V alloy (a) and the selected area electron diffraction patterns of the matrix (b, c, and d).

All the microstructures belonged to Widmanstätten lamellar structures which were related to the inherent anisotropy of the hexagonal crystal structure with dark plates (α phase) and body-centered cubic structure with white regions (β phase). With the increase in the vanadium content of the Ti-*x*V alloy, Widmanstätten lamellar structures became coarser. Coarse β laths were observed much dense at the previous α phase of Ti-15V and Ti-20V alloys (Fig. 3c and 3d). Those laths were inferred to be formed during the etching process with Keller's reagent for metallurgical structure observation, and would reduce the corrosion stability of Ti-10V and Ti-20V alloys.

Fig. 4 shows phase identification revealed by TEM using SAED patterns of Ti-10V alloys. Very fine and irregularly shaped grains were observed in the TEM microstructures of Ti-10V. The SAED patterns from the region marked with an 'A' in the TEM image consisted of a characteristic single crystalline α-Ti phase (Fig. 4b), showing a perfect atomic arrangement, while the SAED pattern acquired from the 'B' region consisted of metastable β-Ti phase, with satellite peaks indicated (Fig. 4c). The SAED patterns of Ti-10V obtained from the 'C' region showed a characteristic single crystalline α-Ti phase (Fig. 4d), which were patterns similar to those of Ti-10V (Fig. 4c). This submicrostructure was due to the formation of a solid solution between vanadium and titanium, which was most likely related to the dominance of hardening effect of Ti-*x*V alloys.

Table 1. Vicker's hardness (VHN), elastic modulus values and ultimate tensile strengths of Ti-*x*V alloys versus cp-Ti for different vanadium contents (number of measurements =5)

Alloy code	Hardness (VHN)	Elastic modulus (GPa)	Ultimate tensile Strength (MPa)
cp-Ti	164.54 (3.54)	114.32 (16.30)	478.19 (21.93)
Ti-5V	433.20 (14.20)	103.75 (6.00)	854.64 (19.73)
Ti-10V	352.00 (33.82)	97.19 (5.12)	881.26 (89.14)
Ti-15V	497.00 (45.09)	84.28 (7.04)	694.29 (189.16)
Ti-20V	379.60 (27.65)	94.53 (5.17)	599.80 (340.74)

The Vicker's hardness numbers (VHNs) for the Ti-*x*V alloys are shown in Table 1. All the Ti-V alloys had significantly higher hardness than the cp-Ti tested ($p<0.05$). The hardness value tended to rise with increasing vanadium content up to 15 wt% and then decreased slightly as the vanadium content increased further. As for the Ti-15V alloy, the microhardness was about 497 VHN. This result indicated that the vanadium element could effectively increase the microhardness values of cp-Ti, which was mainly caused by the solid-solution strengthening of the α-phase and β-phase. The elastic modulus values for Ti-*x*V (x = 5, 10, 15, and 20 wt%) alloys were in the range of 84 to 104 GPa. These values were significantly lower than the value for cp-Ti (114 GPa) ($p<0.05$). For a material to be used as a medical implant, it is advantageous to have an increase in material strength while maintaining a low elastic modulus, since low-modulus material is generally favored for implant application because of its reduced stress shielding effect [17].

The favorable mechanical performance of Ti-*x*V alloys was again confirmed on tensile testing. As indicated in Table 1, the tensile strengths of all four of the Ti-*x*V alloys were much higher than the value for cp-Ti and varied between 600 and 900 MPa for the former, as opposed to 478.19 MPa for cp-Ti. As an example, at Ti-5V, it can be seen that the tensile strength is 854.64 MPa, and this value increases with increasing vanadium content but then decreases after vanadium content exceeds 10% and finally reaches a valley value of 599.80 MPa for Ti-20V.

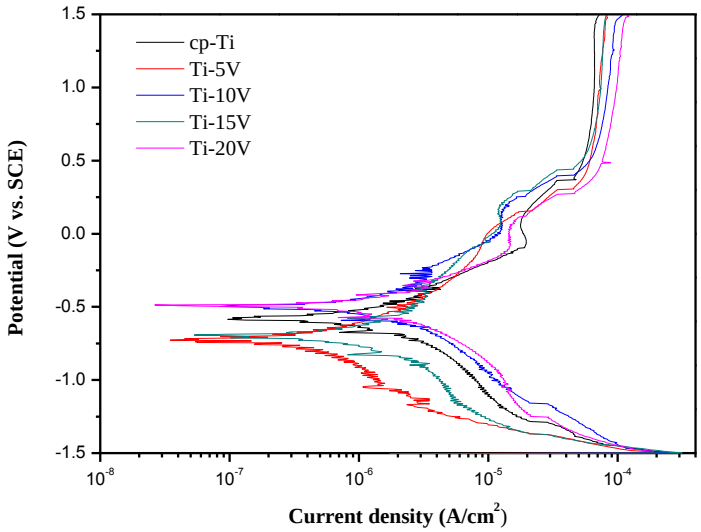

Figure 5. Representative potentiodynamic polarization curves for the cp-Ti and Ti-*x*V alloys.

Table 2. Corrosion potential (E_{corr}) and corrosion current density (i_{corr}) of cp-Ti and Ti-*x*V alloys.

Alloy	E_{corr} (mV vs. SCE)	i_{corr} (μA/cm^2)	β_a	β_c	Corrosion rate (mm/year)
cp-Ti	−550.33 (43.94)	0.611	0.267	0.188	1.88×10^{-2}
Ti-5V	−707.87 (77.12)	0.154	0.173	0.127	0.46×10^{-2}
Ti-10V	−509.50 (48.03)	0.392	0.181	0.158	1.15×10^{-2}
Ti-15V	−627.00 (112.04)	0.325	0.149	0.177	0.93×10^{-2}
Ti-20V	−466.07 (64.34)	0.256	0.101	0.115	0.72×10^{-2}

* Within the same column, mean values with the same superscript letter were not statistically different at 5% ($p>0.05$) by Duncan's multiple range test.

The corrosion behavior of Ti-*x*V alloys was evaluated using potentiodynamic polarization, impedance, and galvanic couple technique in order to investigate the effect of vanadium content on the polarization curve to ascertain its suitability. Potentiodynamic polarization curves of cp-Ti and Ti-*x*V alloys were recorded at a sweep rate of 5 mVs^{-1} between the potential range of −1.5 and +1.5 V in 0.9% NaCl solution, and the results are shown in Figure 5. The curves of Ti-10V and Ti-20V exhibited a positive shift of the electrochemical potential compared with that of cp-Ti. This shift indicated the

positive influence of vanadium on the corrosion resistance of cp-Ti. This is attributed to the promotion of the active-passive transition by the enhanced cathodic reaction [18]. Because the electronegativity of Ti (1.54) is lower than that of V (1.63), electrons move toward the region of V atoms in the alloy. The addition of vanadium promotes oxygen reduction at the cathodic area around the V atoms, and thus the enhanced cathodic reaction accelerates spontaneous passivation of the titanium surface at the anodic area.

The Nyquist and Bode plots of cp-Ti and Ti-V alloys are shown in Fig 6. Ti-V alloys exhibited superior impedance spectra compared with cp-Ti. Among the Ti-V alloys, a dramatic increase in impedance was observed in Ti-5V. Ti-15V showed a higher impedance spectrum as compared with Ti-10V, and Ti-20V displayed the worst impedance performance. Figure 6b shows the relationship of frequency versus phase and the relationship of frequency versus impedance magnitude. The curves in the high frequency range correspond to the resistance of solution, the curves in the middle frequency range correspond to the properties of passive layers, and the curves in the low frequency range correspond to the interface properties between the passive layers and metal surface. The slope of the curves in the middle frequency range versus impedance magnitude showed the capacitive properties of passive layers. Enhanced properties of passive layers of Ti-V alloys were compared with those of cp-Ti. Ti-V alloys had slopes of −0.74 to −0.80 and phases of −65.2 to −75.3°, while cp-Ti had a slope of −0.76 and a phase of −68.7°. Ti-5V exhibited the best properties of passive layers with the minimum phase (−75.3°) and the highest impedance magnitude. Ti-20V with the phase of −65.2° exhibited the lowest properties of passive layers. The optimized equivalent circuits were used to investigate the properties of passive layers. Figure 6c shows the equivalent circuits based on the three passive layer model of cp-Ti and Ti-V alloy. R_s correspond to the resistance of the electrolyte which in the Bode diagram is expressed in a high frequency limit. Q_o and R_o represent the CPEs (constant phase elements) and resistance of the outer porous layer; Q_m, and R_m represent the CPEs and resistance of the intermediate layer; Q_i and R_i indicate the CPEs and resistance of the inner layer. The subscript "o" refers to porous outer layer, "m" refers to intermediate layer, "i" refers to the inner layer. The fitting quality is evaluated by chi-squared (χ^2) values of about 10^{-4} and the fitting results are listed in Table 3.

As listed in Table 3, it is found that the Ti-V alloys have lower capacitance (Q_o, Q_m, Q_i) and higher porous resistance (R_o, R_m, R_i) than that of cp-Ti. The low capacitance and high resistance indicate the formation of a highly stable film on the Ti-V alloys in electrolyte. Therefore, the Ti-V alloys possess a noble electrochemical corrosion behavior, which is consistent with the result of polarization. The low capacitances can be associated with an increase of the passive layer thickness. The enhanced parameters of Ti-V alloys were observed in the intermediate and outer layers. Ti–V alloys exhibited formation of a thicker outer porous layer than cp-Ti. Specially, Ti-5V showed a relatively thick passive outer layer with 35.9 kΩ, others Ti-V alloys displayed similar properties of the outer layer. The good properties of Ti-5V in the intermediate layer and the outer layer resulted in the best corrosion resistance as observed in Figure 6.

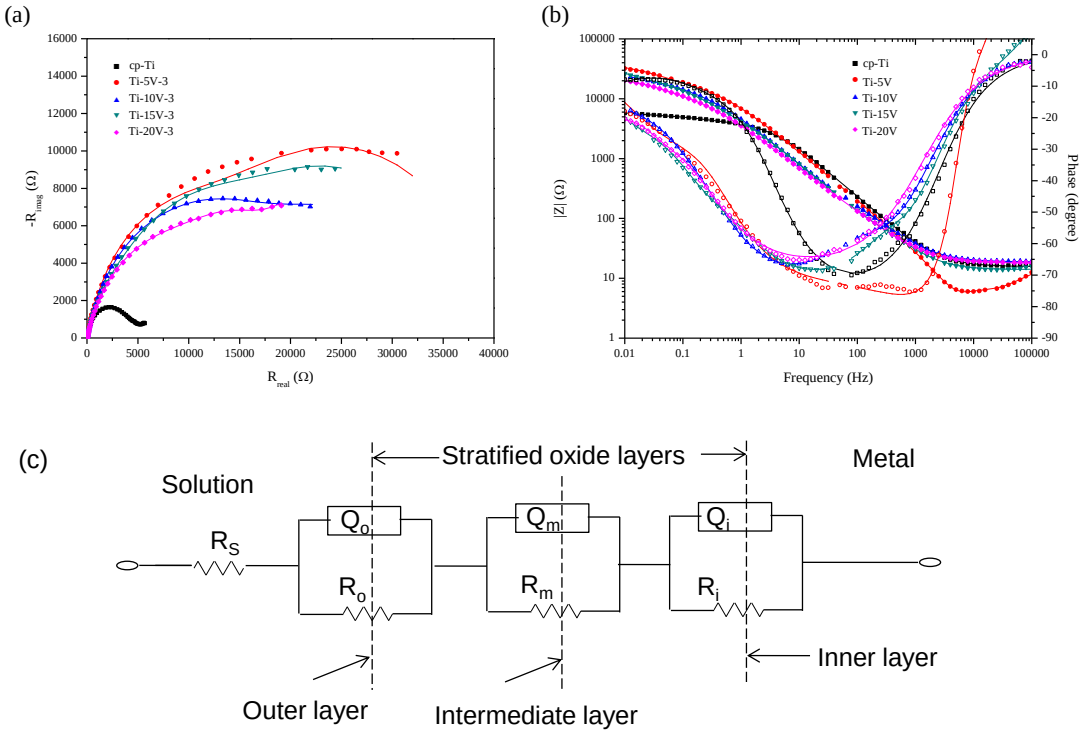

Figure 6. The Nyquist plots (a), Bode plots (b), and equivalent circuit (c) employed in the fitting for cp-Ti and Ti-V alloys in 0.9% NaCl solution.

Table 3. The impedance parameters of cp-Ti and Ti-*x*V alloys in 0.9% NaCl solution.

Sample	**Solution**	**Outer layer**			**Intermediate layer**			**Inner layer**			
	R_S (Ω)	R_o (kΩ)	Q_o (μS·s^{no})	n_o	R_m (kΩ)	Q_m (μS·s^{nm})	n_m	R_i (kΩ)	Q_i (μS·s^{ni})	n_i	χ^2 (10^{-4})
cp-Ti	15	2.53	2370	0.76	7.62	4220	0.78	2.55	183	0.80	1.83
Ti-5V	232	35.9	127	0.52	15.8	24.0	0.86	12.0	843	0.91	3.26
Ti-10V	16	13.4	594	0.80	13.1	297	0.84	6.70	2620	0.92	1.69
Ti-15V	19	17.0	203	1.00	16.0	529	0.83	12.4	455	0.78	1.66
Ti-20V	18	10.3	123	0.81	12.6	1190	0.80	13.0	935	0.91	1.54

*S means siemens and s represents seconds.

Figure 7 presents the galvanic currents versus time of the couplings of cp-Ti/Ti-*x*V alloys in 0.9% NaCl solution at 37°C. All the Ti-*x*V alloys apparently behaved in a similar manner. Current values initially showed a steep decrease and then a leveling off. This general behavior might be explained by the reduction in the active area due to the growth of a passive film on the surface of cp-Ti. A steady-state current value was attained more rapidly for Ti-5V and Ti-10V than for cp-Ti, indicating that the passive film grew more rapidly on cp-Ti. The time required for the Ti-*x*V alloys to attain a constant current was increased as the vanadium content increased.

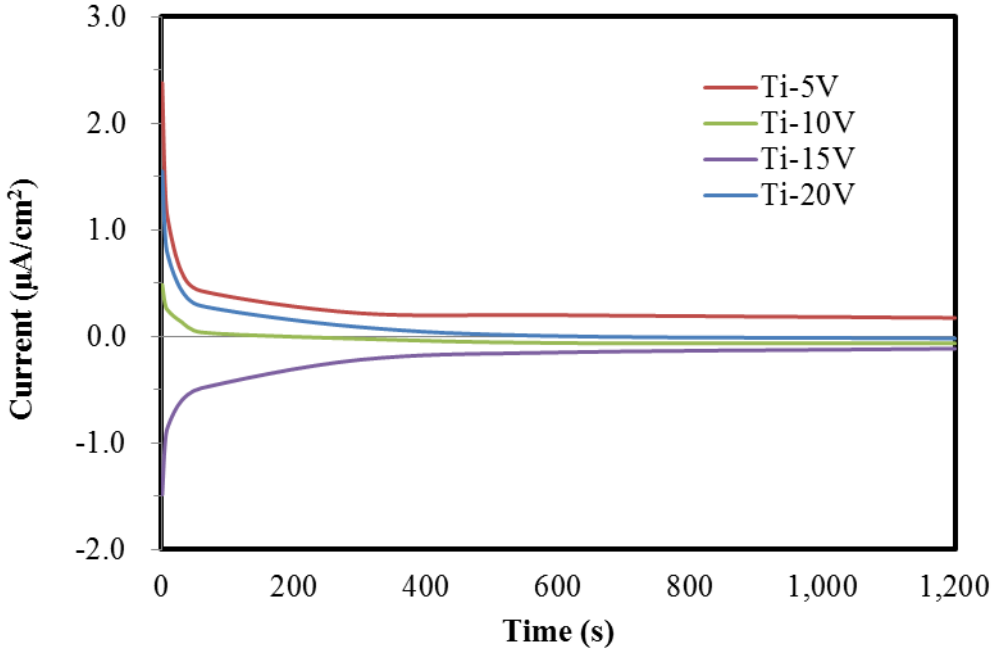

Figure 7. Mean values of galvanic currents versus time of the couplings of cp-Ti/Ti-*x*V alloys.

4. CONCLUSIONS

We prepared a series of Ti-*x*V alloys with vanadium contents ranging from 5 to 20 wt% and investigated the effects of the addition of vanadium on microstructure, mechanical properties, corrosion behavior of Ti alloys. In the Ti-10V alloy, the microstructure consisted of α-Ti and β-Ti phases. By alloying with vanadium, the cast Ti-*x*V alloys exhibited improved hardness. The enhanced mechanical properties of the Ti-*x*V alloys could be induced from the formation of solid solution between vanadium and titanium. It was found that Ti-*x*V showed better corrosion resistance and higher oxidation protection ability than cp-Ti. Considering all the mechanical properties and corrosion behaviors, the Ti-*x*V alloy with vanadium contents of 5 wt% could be a good candidate for dental casting alloys.

ACKNOWLEDGMENTS
This work was supported by Chonnam National University (2015), and by the National Research Foundation of Korea (NRF) grant funded by the Korea government (MSIP) (No. 2011-0030121).

References

1. A.T. Sidambe, *Materials*, 7 (2014) 8168-8188.
2. C.J. Hu and J.R. Lu, *Int. J. Electrochem. Sci.*, 10 (2015) 749 – 758.
3. F.J. Gil, L. Delgado, E. Espinar and J.M. Llamas, *J. Mater. Sci. Med.*, 23 (2012) 885-890.

4. D. Mareci, R. Chelariu, G. Bolat, A. Cailean, V. Grancea and D. Sutiman, *Trans. Nonferrous Met. Soc. China*, 23(2013) 3829−3836.
5. D.C. Crans, J.J. Smee and E. Gaidamauskas and L. Yang, *Chem. Rev.*, 104 (2004) 849–902.
6. W.F. Ho, W.K. Chen, S.C. Wu and H.C. Hsu, *J. Mater. Sci-Mater. M.*, 19 (2008) 3179−3186.
7. Y. Okazaki and E. Gotoh, *Biomaterials*, 26 (2005) 11−21.
8. D.A. Barrio and S.B. Etcheverry, *Can. J. Physiol. Pharmacol.*, 84 (2006) 677–686.
9. M. Anke, *Anal. Real Acad. Nac. Farm.*, 70 (2004) 961–999.
10. J.C. Bailar, H. J. Emelelus, R. Nyholm and A.F. Trotman-Dickenson, *Comprehensive Inorganic Chemistry*, Pergamon Press, Vol. 3 (1973) 491-551.
11. J.F. Smith and K.J. Lee, Binary Alloy Phase Diagrams, Second Edition, Vol. 3, T.B., Massalski (Editor-in-Chief), Materials Information Soc., Materials Park, Ohio (1990).
12. Metal-ceramic dental restorative systems, ISO 9693, International Organization for Standardization, Geneva, Switzerland, 1999.
13. Standard reference test method for making potentiostatic and potentiodynamic anodic polarization measurements, ASTM G5-94, 2004.
14. Standard practice for verification of algorithm and equipment for electrochemical impedance measurements, ASTM G106-89, 2010.15. Joint Committee on Powder Diffraction Standards (JCPDS), International Centre for Diffraction data, PA, USA, 1995.16. J.H. Cho, M.J. Hwang, M.K. Han, O.S. Han, H.J. Song and Y.J. Park, *J. Alloy. Compd.*, 610 (2014) 74–81.
17. M. Geetha, A.K. Singh, R. Asokamani and A.K. Gogia, *Prog. Mater. Sci.*, 54 (2009) 397–425.
18. X.Q. Wu, Q.Peng, J.C. Zhao and J.G. Lin, *Int. J. Electrochem. Sci.*, 10 (2015) 2045 – 2054.